Available online at www.sciencedirect.com

SciVerse ScienceDirect

Ceramics International 39 (2013) 2405–2414

CERAMICS INTERNATIONAL

www.elsevier.com/locate/ceramint

Fatigue and subcritical crack growth in ZrO_2–bioglass ceramics

L.A. Bicalho[a], C.A.R.P. Baptista[a], R.C. Souza[b], C. Santos[a,c,*], K. Strecker[d], M.J.R. Barboza[a]

[a]*Departamento de Engenharia de Materiais, Universidade de São Paulo-Escola de Engenharia de Lorena, EEL-USP, Pólo Urbo-Industrial, Gleba AI-6, s/n, Lorena, SP, Brazil*

[b]*Área de Mecânica, Instituto Federal de São Paulo-Campus São João da Boa Vista, IFSP-SJBV, Acesso Dr. João Batista Merlin, s/no-Jd Itália, S. J. B. Vista, SP, Brazil*

[c]*Pró-Reitoria de Pesquisa e Extensão, UNIFOA—Centro Universitário de Volta Redonda Av. Paulo Erlei Alves Abrantes, 1325 Três Poços, V.Redonda, RJ, Brazil*

[d]*Universidade Federal de São João Del Rey, Departamento de Mecânica, UFSJ-DEMEC, Praça Frei Orlando, 170, Centro, São João Del Rei, MG, Brazil*

Received 25 June 2012; received in revised form 24 August 2012; accepted 24 August 2012
Available online 26 September 2012

Abstract

This work investigates the characteristics of ZrO_2 based ceramics (Y-TZP) doped with bioglass developed for dental prostheses. Powder mixtures composed of zirconia and 3 or 5 wt% of $3CaO \cdot P_2O_5$–SiO_2–MgO bioglass were sintered at 1300 °C for 2 h. The samples were characterized by their phase composition using X-Ray diffraction (XRD) and analysis of their microstructure by scanning electronic microscopy (SEM). Hardness and fracture toughness were evaluated using the Vickers indentation method, while bending strength and fatigue resistance were determined using the four-point bending testing. The mechanical properties indicate that the samples achieved high density under the applied sinter conditions. X-ray diffraction analysis revealed tetragonal ZrO_2 as a major crystalline phase. Hardness, fracture toughness and bending strength of the sintered samples containing 3% or 5% bioglass were 1167and 1134 HV, 6.3 and 6.1 MPa $m^{1/2}$ and 453 and 636 MPa, respectively. The fatigue results presented large scattering, which is attributed to a heterogeneous distribution of the secondary glassy phase in the zirconia matrix. The non-uniform dispersion of the glass may result in the formation of stress gradients, possibly responsible for crack initiation and their respective subcritical growth during fatigue testing. The fatigue limit determined was superior to stresses developed during mastication, turning its use in dental prostheses viable. Weibull statistics were applied on the fatigue results obtained at average stress levels of 255, 270 and 285 MPa in order to calculate the subcritical crack growth. A life expectancy of over 20 years under severe cyclic pressure conditions has been calculated.

Keywords: C. Fatigue; Zirconia; Bioglass; Subcritical crack growth

1. Introduction

Metal alloys are currently used as crown or abutment materials in bone-integrated implant fixtures like dental prostheses. The material ought to be biocompatible and must not promote plaque adherence, besides providing sufficient strength to endure and transmit occlusal forces to the implant and supporting the bone. Another significant factor is esthetics, in order to approach the visible aspect of natural tooth. All these properties are essential for intra-oral applications [1–3]. An important improvement has been possible by the use of "all-ceramic" systems.

All-ceramic dental restorations are attractive to the dental community because they provide higher strength and abrasion resistance, better biocompatibility and esthetics, when compared with metal and resin restorations [2,4]. On the other hand, the application of all-ceramic crowns and bridges is limited by their brittle behavior, long processing time and machinability performance [5,6]. The most widely used ceramic materials are lithium disilicate ($Li_2Si_2O_5$), alumina (Al_2O_3) and zirconia (ZrO_2) [7]. These are important dental ceramics due to their excellent biocompatibility. The main advantages of Al_2O_3 are its

*Corresponding author at: Departamento de Engenharia de Materiais, Universidade de São Paulo-Escola de Engenharia de Lorena, EEL-USP, Pólo Urbo-Industrial, Gleba AI-6, s/n, Lorena, SP, Brazil.
Tel.: +55 12 31599926; fax: +55 12 31533006.
E-mail address: claudinei@demar.eel.usp.br (C. Santos).

0272-8842/$ - see front matter © 2012 Elsevier Ltd and Techna Group S.r.l. All rights reserved.
http://dx.doi.org/10.1016/j.ceramint.2012.08.093

high hardness and wear resistance, while $Li_2Si_2O_5$ and ZrO_2 exhibit higher fracture strength and fracture toughness, and lower Young's Modulus [8–10]. It has been known that the t→m (tetragonal–monoclinic) crystalline phase transformation in pure undoped zirconia during cooling is a reversible, athermal martensitic transformation, associated with a finite amount of volume change of 3–5% [6]. This leads to crumbling of a sintered part made out of pure zirconia. Several additives, such as Y_2O_3, CeO_2, MgO, etc., are usually added to stabilize the tetragonal phase in the sintered microstructure.

Tetragonal zirconia polycrystals (TZP) with 3 mol% Y_2O_3 (3Y-TZP) are usually fabricated by solid-state sintering at temperatures around 1550–1600 °C [6,8–10], an expensive fabrication method that inevitably increases production costs and limits their utilization. Sometimes, in order to decrease the sintering temperature, additives are deliberately introduced.

Recently, many studies have been reported concerning the effects of additives on the sintering and the resulting mechanical properties of zirconia ceramics [11–14]. The possibility of combining the good mechanical and biological properties as well as the thermal compatibility of bioglasses from the system $3CaO \cdot P_2O_5$–SiO_2–MgO [15,16] with the properties of tetragonal ZrO_2, allows for the reduction of production costs and to glimpse an increase of the application field of these materials, especially as part of a dental implantation such as abutment.

Cyclic fatigue of ceramics recently became a highly attractive research field for material scientists. There is a strong demand to generate design-relevant fatigue data which are required for many of the projected applications of structural ceramics as dental materials. On the other hand, knowledge of fatigue in ceramics is insufficient so far and information about the correlation between microstructural parameters and fatigue properties is still missing for most ceramic systems. Besides this lack of understanding, a number of fundamental questions still have not been answered unambiguously for many of the most important ceramics [17–20]. The purpose of this study is to evaluate the cyclic fatigue life of ZrO_2–bioglass ceramics sintered at low temperatures, correlating their properties with the densification and the fraction of monoclinic-ZrO_2 phase.

2. Experimental procedure

2.1. Processing

High-purity ZrO_2-(3 mol%Y_2O_3) powder containing 15 vol% of residual ZrO_2-monoclinic phase (Tosoh Grade 3YSB-Japan) and bioactive $3CaO \cdot P_2O_5$–SiO_2–MgO (52.75 wt%–3 $CaO \cdot P_2O_5$, 30 wt%–SiO_2 and 17.25 wt%–MgO) glass powder were used as starting powders. The bioactivity of this glass was studied by Oliveira et al. [15,16]. The powder mixtures, containing 3 or 5 wt% of bioglass, were milled and homogenized to a size of 32 μm. Specimen were compacted by cold uniaxial pressing at 80 MPa for 60 s. The green compacts with a relative green density of approximately 55% of the theoretical density were sintered at 1300 °C, in a $MoSi_2$ furnace for 2 h, with heating and cooling rates of 10 °C/min.

2.2. Characterization

Bulk density, and consequently, relative density, were measured by the Archimedes method in distilled water. The crystalline phases were determined by X-ray diffractometry (XRD) using Cu-Kα radiation in the 2θ range of 20–80°, with a 0.05° step width and 3 s exposure time per position. The monoclinic-ZrO_2 phase fraction was calculated using the *Garvie and Nicholson* method [21]. The thermally etched surfaces of the samples were examined by scanning electron microscopy—LEO-1450VP microscope. Between 1000 and 1200 grains of each sample were measured using the software by LEICA Qwin-Image Processing and Analysis System for determination of the average grain size.

2.3. Mechanical properties

The hardness and fracture toughness were determined by Vickers' Indentation Method, under an indentation load of 2000*g*F, for 30 s.

Polished rectangular bars of $4 \times 3 \times 45\ mm^3$ were prepared according ASTM C 1116-94, for the determination of the bending strength using a four-point bending device with outer and inner spans of 40 and 20 mm, respectively, at a crosshead speed of 0.5 mm/min, using a MTS 310 Universal Test Machine.

The cyclic fatigue tests were carried out by four-point bending loading in air at room temperature, under a relative humidity of about 60%. The specimen dimensions and the testing machine were the same as employed in the bending strength tests. The cyclic fatigue behavior was studied under a sinusoidal stress wave form with a frequency of 25 Hz and a constant stress ratio (min/max) $R=0.1$. The minimum number of specimens used in the fatigue tests was 11 samples for each stress level. The tests were interrupted when the samples survived more than 2×10^6 stress cycles.

The static bending strength of the samples in question was described by Weibull [22] statistics, using the following equation:

$$F(\sigma_C) = 1 - \exp\left(-\frac{\sigma_C}{\sigma_{C,0}}\right)^m \quad (1)$$

where 'F' is the probability of failure; σ_C, is the static bending strength; $\sigma_{C,0}$, is the characteristic strength of a failure probability of approximately 63% and 'm' is the Weibull modulus. The failure probability was calculated assuming the unbiased estimator: '$F_i=(i-0.5)/t$', where 'F_i' is the probability of failure of the 'ith' sample and 't' the total number of samples tested.

The fatigue life results (N_f) obtained from cyclic bending tests were also described using Weibull statistics. In this case, for each stress level a characteristic life $N_{f,0}$ and the fatigue Weibull modulus m^* are determined by using an expression similar to Eq. (1).

Results and discussions arising from this study are organized as follows. First, results of the mechanical strength under static and fatigue life are presented in the form of charts and the Weibull distribution parameters are determined using 11 samples of each composition with 3% or 5% of bioglass, referred to as '97:03' and '95:05', respectively. This analysis was applied to the results obtained at stress levels of 255, 270 and 285 MPa. The information provided in these charts was used to calculate the fatigue and subcritical crack growth parameters for the stresses to which the studied materials were subjected. Finally, curves of subcritical crack growth, which display the crack propagation rate as a function of the stress intensity factor, were determined based on the Weibull data, as proposed by Studart et al. [23,24].

3. Results and discussion

3.1. Phase analysis

The phase analysis of the sintered samples by X-Ray diffraction, shown in Fig. 1, indicates the presence of a small amount of residual monoclinic phase, besides the tetragonal ZrO_2 phase. Further crystalline phases were not detected in any sintered specimen, indicating that the bioglass added is either fully amorphous or else the fractions present in the sintered samples are below the detection limit of the diffractometer.

3.2. Evaluation of microstructures

Fig. 2 shows representative micrographs of sintered Y-TZP samples with 3% or 5% bioglass. In both cases the observed microstructures were quite similar, showing equiaxed grains of ZrO_2 with an average grain size of about 0.3 μm. The microstructural parameters, average grain size and grain density per area, obtained from the micrographs shown in Fig. 2, are presented in Table 1 and allow to verify whether the presence of liquid phase formed by the added bioglass interfered in the grain growth of ZrO_2. By analyzing the results in Table 1, it can be stated that the amount of bioglass added has a negligible

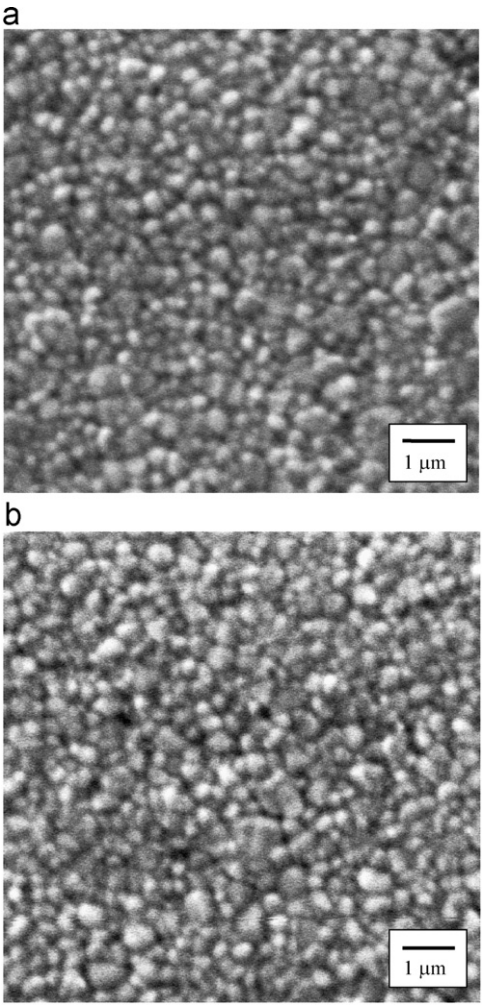

Fig. 2. Micrographs of 3Y-TZP with (a) 3% and (b) 5% bioglass addition, sintered at 1300 °C.

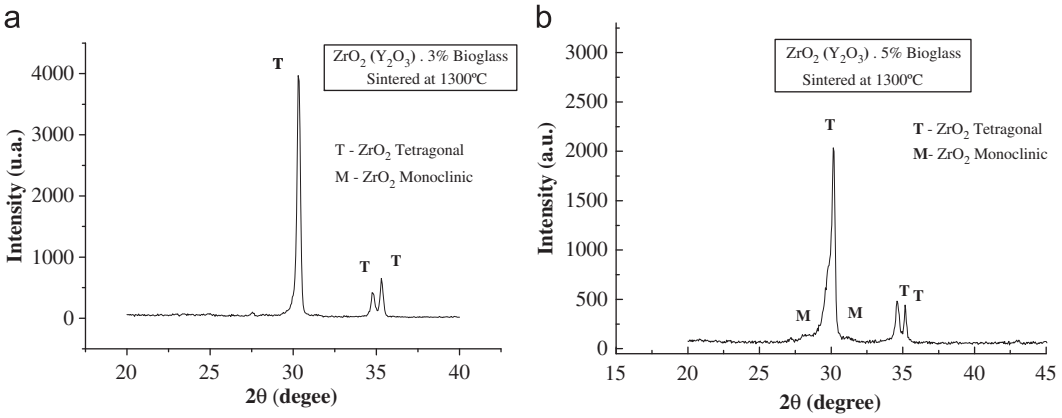

Fig. 1. X-Ray diffraction patterns of 3Y-TZP with (a) 3% and (b) 5% bioglass addition, sintered at 1300 °C.

influence on the average grain size of ZrO_2 and the density of grains per unit area.

These microstructural characteristics are a direct function of the initial grain size and the sintering temperature used. Dense Y_2O_3-stabilized ZrO_2 is usually obtained by solid state sintering at temperatures of about 1500 °C. It was observed that, at this temperature [6,11], the average grain size may vary from 0.5 μm to 1 μm, depending on the sintering time. The use of a relatively low sintering temperature such as 1300 °C reduces grain growth, thus increasing the grain population per unit area. In this study, one of the goals using a liquid phase has been to facilitate densification at lower temperatures, and, at the same time, to reduce grain growth. Smaller grains combined with an intergranular fracture mode should hinder the growth and propagation of cracks during the fracture. Furthermore, smaller grains lead also to the beneficial effect known as transformation toughening by the martensitic t→m ZrO_2 phase transformation [6].

Table 1
Microstructural parameters of the 3Y-TZP–bioglass materials, sintered at 1300 °C.

$ZrO_2(Y_2O_3)$: Bioglass (wt%)	Average grain size (μm)	Density of grains (No. grains/μm^2)
97:03	0.325 ± 0.065	9.982
95:05	0.329 ± 0.076	9.964

Table 2
Vickers hardness, fracture toughness and flexural strength of the sintered samples.

$ZrO_2(Y_2O_3)$: Bioglass (wt%)	Vickers hardness (HV_{2000gF})	K_{IC} (MPa m$^{1/2}$)	Flexural strength (MPa)
97:03	1167 ± 80	6.3 ± 0.2	453 ± 74
95:05	1134 ± 76	6.1 ± 0.4	363 ± 54

3.3. Mechanical properties

Table 2 presents the results of the Vickers hardness and fracture toughness (K_{IC}) for both compositions studied, as well as the bending strength determined from four-point bending tests.

The samples containing 3 wt% of bioglass (97:03) showed a discrete increase, near 3%, in hardness and a similar fracture toughness than samples sintered with 5 wt% of bioglass (95:05). This slight difference in hardness is probably due to the smaller amount of intergranular phase, because both compositions present full relative density after sintering.

The bending strength of sintered samples containing 3 wt% glass (450 MPa) is almost 25% higher compared to samples containing 5 wt% glass (360 MPa). This result is attributed to the lower strength of the glass compared to zirconia, thus higher amounts of secondary glassy phase result in lower strength. Furthermore, the concentration of glass in pockets, may also weaken the material.

3.4. Fatigue resistance

The fatigue results of the Y-TZP/bioglass materials are presented in Fig. 3, plotting the number of cycles as a function of the applied stress range. For samples that did not fail within the range of $2–5 \times 10^6$ cycles the test was stopped (run-out) and infinite life was assumed. These charts also reveal distinct behaviors among the tested compositions. While for specimen '97:03' it is possible to observe a tendency of an increasing fatigue life under lower applied stresses. For specimen '95:05' the experimental data are more dispersed but can be divided into two categories, whatever the applied stress, samples that failed with a very low number of cycles and samples that showed a tendency to infinite life.

The fracture surfaces of the fatigued specimens allow the observation of crack nucleation sites, as well as the

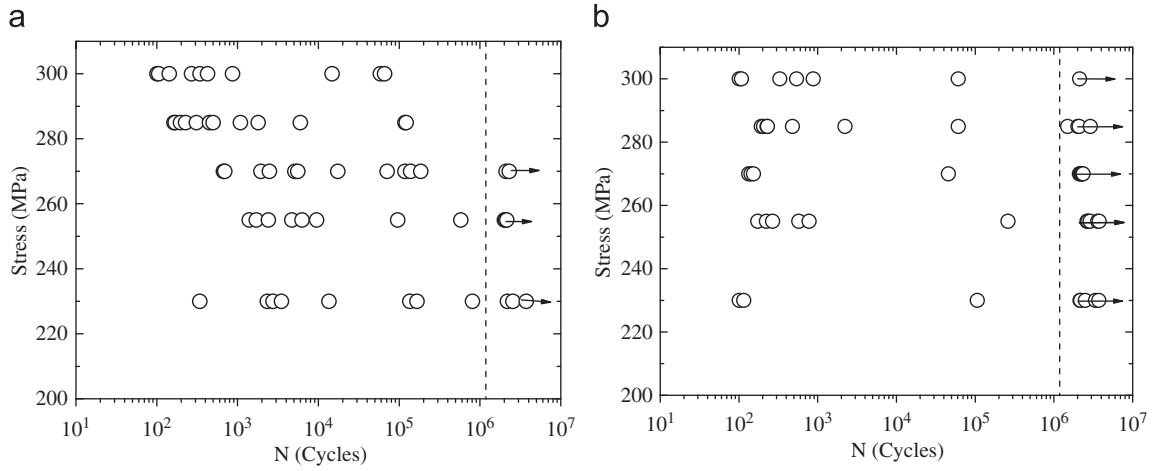

Fig. 3. Fatigue test results (σ_{max} vs. N) for 3Y-TZP containing (a) 3 wt% and (b) 5 wt% bioglass.

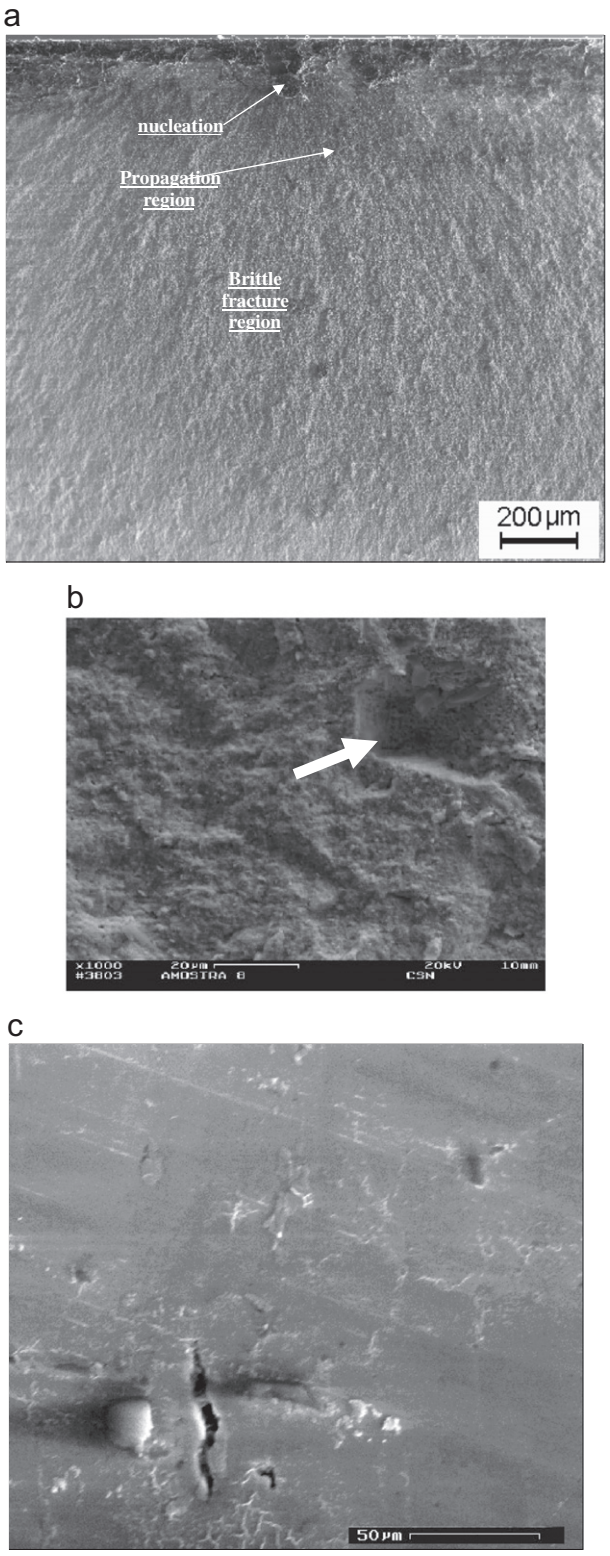

Fig. 4. *Post Mortem* analysis: (a) typical fatigue fracture surface (97:03, 255 MPa, 5.8×10^5 cycles); (b) presence of voids leading to a decrease in fatigue resistance (95:05, 285 MPa, after 4×10^4 cycles); (c) arrested surface crack (95:05, 285 MPa, run-out after 5×10^6 cycles).

subcritical and final crack propagation regions, as shown in Fig. 4a for a 97:03 specimen fractured after 5.8×10^5 cycles. Lower fatigue lives can be related to the presence of micrometric defects produced in processing steps. These flaws, for example as shown in Fig. 4b, may have dimensions as large as 20 µm, much larger than the average grain size of the material, acting as stress concentrators. The scattering of the fatigue results is increased by the presence of these flaws in some of the specimens. The experimental results indicate that the '95:05' material is more susceptible to defect-induced premature failures. The polished surfaces of some specimens after run out exhibited arrested transverse cracks, as shown in Fig. 4c. This behavior is attributed to the transformation toughening mechanism by the tetragonal to monoclinic phase transformation of ZrO_2 ahead of the crack tip.

3.5. Subcritical crack growth

In this section, two distinct methods are employed in order to estimate the crack growth behavior during cyclic

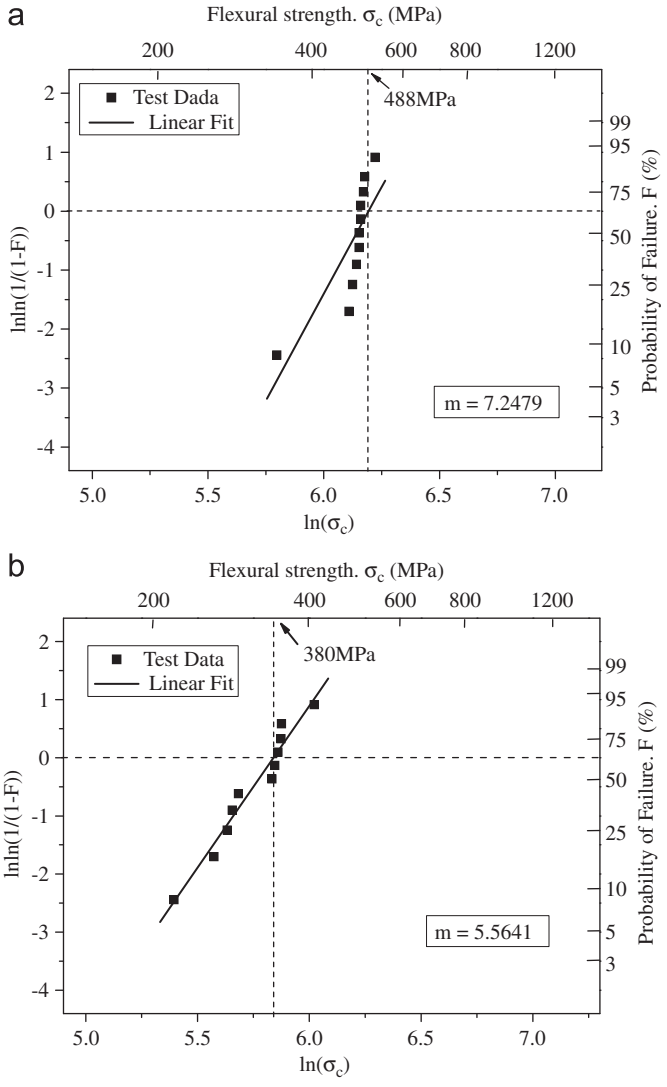

Fig. 5. Weibull distribution of static flexural strength for 3Y-TZP containing (a) 3 wt% and (b) 5 wt% bioglass.

loading in the ZrO_2–bioglass ceramics studied in this work. Both methods use the statistical analysis of the bending strength and fatigue life to calculate the fatigue crack growth rate as a function of the stress intensity factor as defined by the linear elastic fracture mechanics. The first method, proposed by Studart et al. [23,24], is described as follows.

The Weibull analysis of the static strength data of the materials studied in this work is shown in Fig. 5. The Weibull parameters 'm' and '$\sigma_{C,0}$' of Eq. (1) were obtained from the slope of the interpolated straight lines and the intercepts corresponding to $lnln\,(1/(1-F))=0$, respectively, see Table 3. These results show that specimen of composition '97:03' exhibit a higher characteristic strength $\sigma_{C,0}$ and also a narrower scattering of the strength data, as indicated by the higher Weibull modulus m in comparison to specimen of composition '95:05'. The results of '$\sigma_{C,0}$' and 'm' are employed in Eqs. (5) and (6), for the calculation of the subcritical crack growth parameters.

Table 3
Weibull parameters of static flexural strength data.

$ZrO_2(Y_2O_3)$:Bioglass (wt%)	$\sigma_{C,0}$ (MPa)	m
97:03	488	7.25
95:05	380	5.56

The Weibull statistics of the fatigue life data are shown in Figs. 6–8 and Table 4. Maximum stress levels of 255, 270 and 285 MPa were chosen in order to perform the subcritical crack growth calculations. In order to do so, 11 fatigue tests were performed for each material composition and each stress level and the Weibull parameters 'm^*' and '$N_{f,0}$' were obtained in a similar way as the parameters of Eq. (1).

Figs. 6–8 and Table 4 confirm that the fatigue life data of the '95:05' composition is more scattered than those of the '97:03' material. However, the higher number of

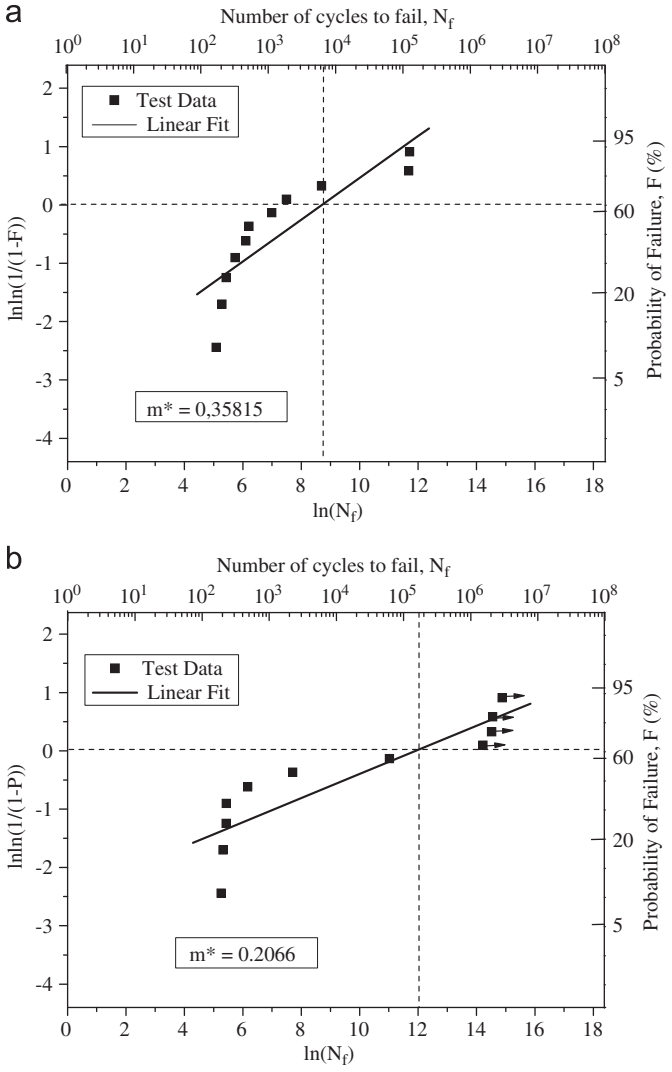

Fig. 6. Weibull distribution of the number of cycles to failure under cyclic stress of 285 MPa, for 3Y-TZP containing (a) 3 wt% and (b) 5 wt% bioglass.

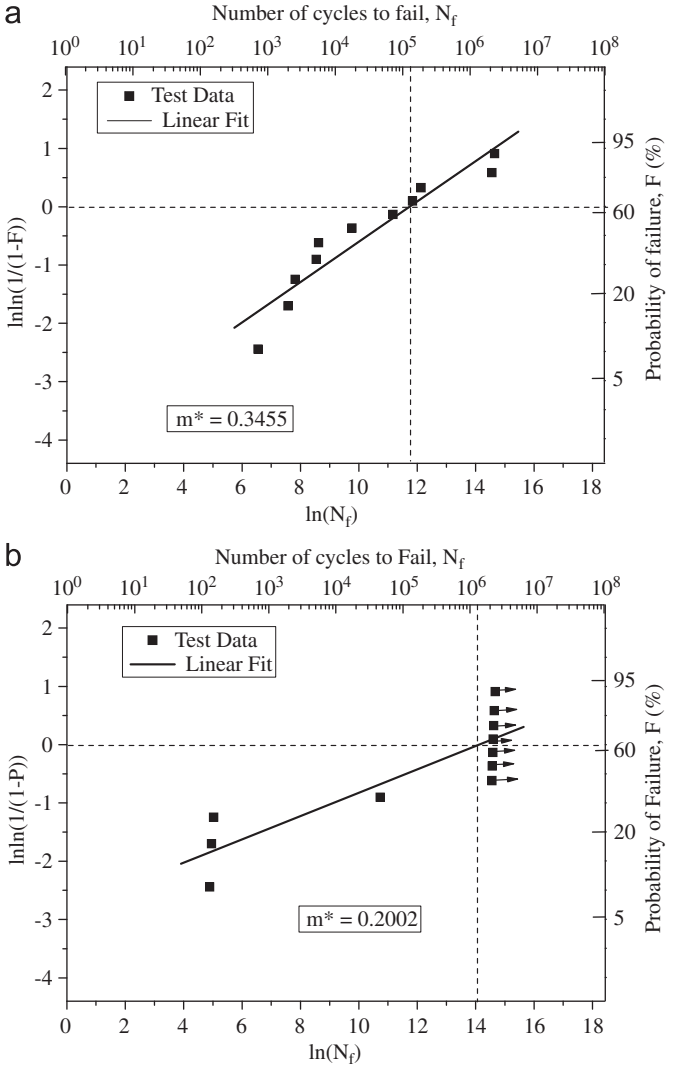

Fig. 7. Weibull distribution of the number of cycles to failure under cyclic stress of 270 MPa, for 3Y-TZP containing (a) 3 wt% and (b) 5 wt% bioglass.

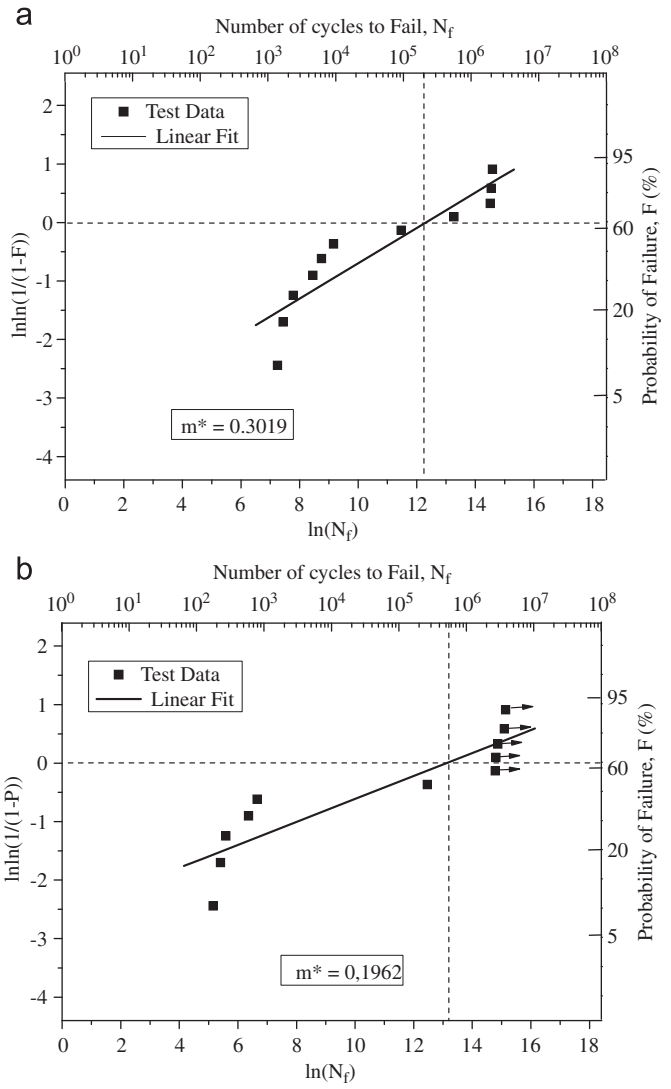

Fig. 8. Weibull distribution of the number of cycles to failure under cyclic stress of 255 MPa, for 3Y-TZP containing (a) 3 wt% and (b) 5 wt% bioglass.

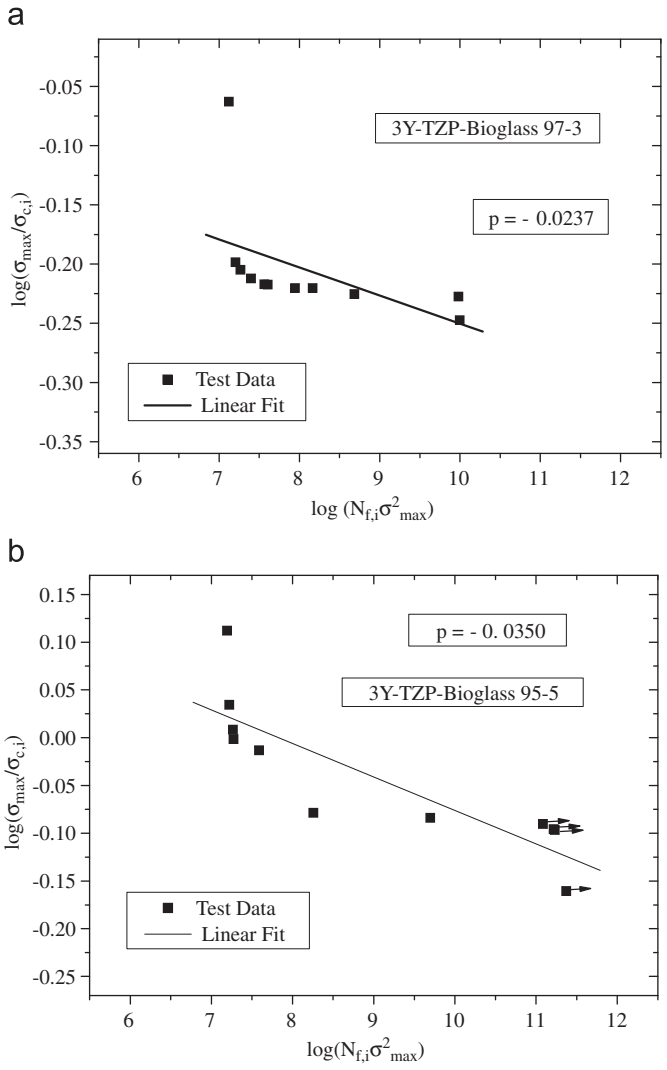

Fig. 9. Auxiliary diagram used in the calculation of the subcritical crack growth under a cyclic stress of 285 MPa, for 3Y-TZP with (a) 3 wt% and (b) 5 wt% bioglass.

Table 4
Weibull parameters of cyclic fatigue life data.

Nominal stress (MPa)	$N_{c,0}$ (cycles)		m^*	
	97:03	95:05	97:03	95:05
285	6,073	152,234	0.3581	0.2066
270	133,168	1,454,972	0.3455	0.2002
255	223,988	524,878	0.3019	0.1962

run-outs of the former lead to higher $N_{f,0}$ numbers, indicating that this composition would be more resistant to cyclic loading. As shown in Fig. 4, microstructural defects related to an inhomogeneous phase distribution, i.e. the occurrence of bioglass pockets that may act as flaws, are responsible for the higher scattering observed in the '95:05' data.

Fatigue and subcritical crack growth in materials subjected to cyclic loading, are usually described by the empirical 'Paris Law', which correlates the crack growth rate 'v' with the applied stress intensity factor as follows, Eq. (2):

$$v = A(\Delta K_I)^n \quad (2)$$

where 'n' and 'A' are the parameters of subcritical crack growth under cyclic fatigue and 'ΔK_I' is the range of the applied stress intensity factor given by ($K_{I,\max} - K_{I,\min}$), '$K_{I,\max}$' and '$K_{I,\min}$' being the maximum and minimum stress intensity factor values in a given loading cycle respectively. In the case of cyclic loading, the crack velocity 'v' is given by the rate of change of the increment in crack length (da) in relation to the number of applied cycles (dN): 'da/dN'.

In the case of polycrystalline ceramics such as 3Y-TZP, the crack growth rate under cyclic loading exhibits a

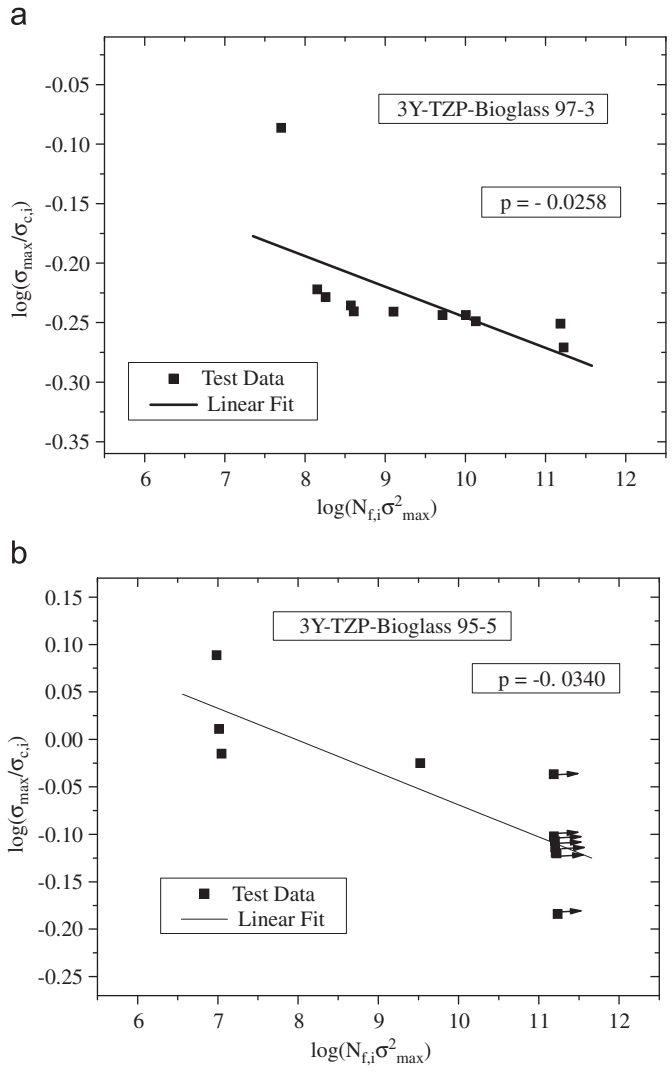

Fig. 10. Auxiliary diagram used in the calculation of the subcritical crack growth under a cyclic stress of 270 MPa, for 3Y-TZP with (a) 3 wt% and (b) 5 wt% bioglass.

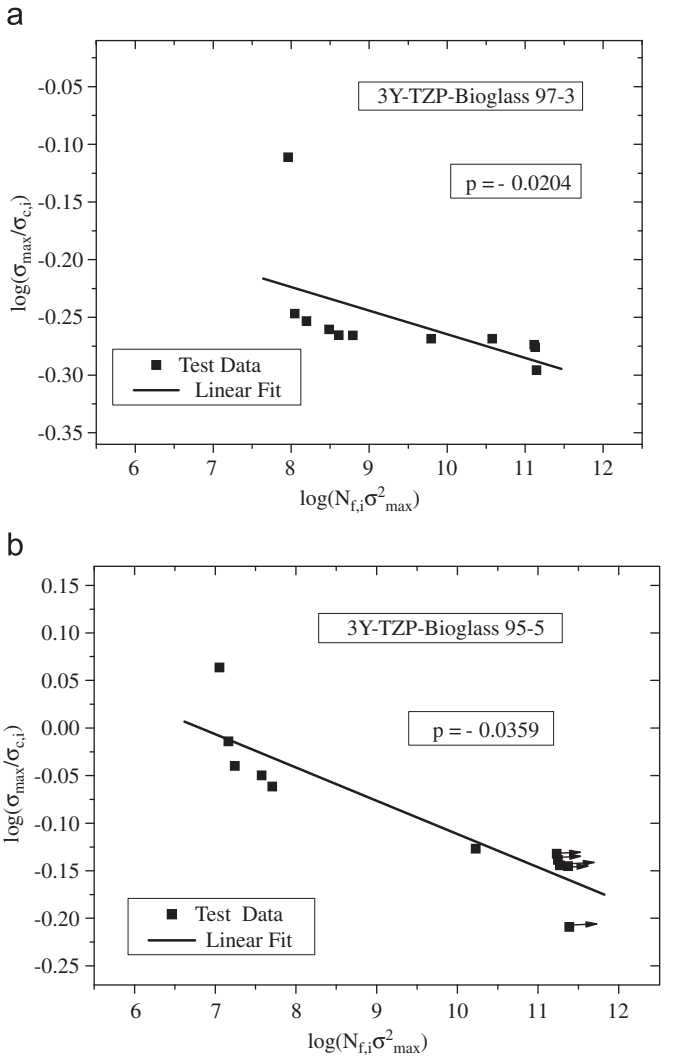

Fig. 11. Auxiliary diagram used in the calculation of the subcritical crack growth under a cyclic stress of 255 MPa, for 3Y-TZP with (a) 3 wt% and (b) 5 wt% bioglass.

stronger dependence on the maximum stress intensity factor '$K_{I,\max}$' than on the stress range 'ΔK_I' [26,27]. Other empirical equations, which deal specifically with this issue, have thus been proposed to describe the fatigue behavior of polycrystalline ceramics [26,27]. Because these equations have not been applied to other polycrystalline materials yet, the fatigue behavior of dental ceramics is evaluated in this paper in terms of the simpler Eq. (3), proposed by Munz and Fett [25]:

$$v = A(1-R)^n(K_{I,\max})^n = A^*(K_{I,\max})^n \quad (3)$$

where 'R' is the stress intensity ratio "$K_{I,\min}/K_{I,\mathrm{Max}}$" and '$A^*$' is the parameter of subcritical crack growth under cyclic fatigue. The value of '$K_{I,\max}$' is directly related to the maximum stress '$\sigma_{\max}$', according to Eq. (4) [25]:

$$K_{I,\max} = \sigma_{\max}\Psi\sqrt{a} \quad (4)$$

where Ψ is a geometrical factor that depends on crack location and shape, and is assumed in the present work to be 1.3, according to results for elliptical surface cracks, as reported by Studart et al. [28].

The Weibull distribution parameters of flexural strength and fatigue life, given in Tables 3 and 4, were used to calculate the subcritical crack growth parameters 'A^*' and 'n', according to Eqs. (5) and (6) [23,24]. The calculations were performed using the previously reported values of K_{IC} of 6.3 MPa $m^{1/2}$ for the material '97:03' and 6.1 MPa $m^{1/2}$ for the material composition '95:05'.

$$A^* = \frac{2K_{\mathrm{IC}}^{2-n}\sigma_{C,0}^{n-2}}{N_{f,0}\Psi^2}(n-2)(\sigma_{\max})^n \quad (5)$$

$$n = \frac{m}{m^*} + 2 \quad (6)$$

The second method, proposed by Munz and Fett [25], can be used for this purpose assuming that the group of monotonically tested samples contains a similar defect size distribution as the samples subjected to fatigue life experiments. The method requires an auxiliary diagram to be

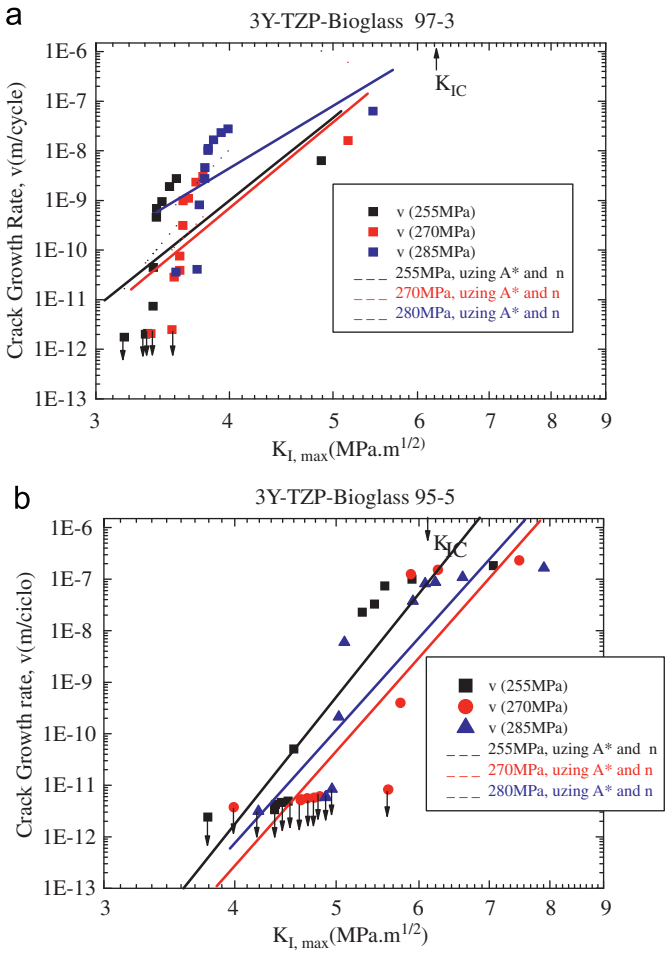

Fig. 12. Crack growth rate (v) as a function of the fracture toughness, $K_{I,\max}$, for samples of 3Y-TZP–Bioglass, under cyclic loading.

initially plotted. To do so, the flexural static strength results ($\sigma_{c,i}$, experimental points shown in Fig. 5) and the number of cycles obtained from the fatigue tests ($N_{f,i}$, experimental points of Figs. 6–8) are ranked and normalized in relation to the respective maximum stress applied in the fatigue test, $\sigma_{\max}$. Figs. 9–11 show the auxiliary diagrams in the form of $\log(\sigma_{\max}/\sigma_{c,i})$ *versus* $\log(N_{f,i}.\sigma^2_{\max})$ plots. The slopes of the linear fits from these diagrams, denoted by 'p', are employed in the fatigue crack growth rate calculations, which are performed according to Eq. (7) for each pair of ranked experimental points.

$$v_i = -\frac{2pK_{IC}^2}{N_{f,i}\sigma_{c,i}^2 Y^2} \tag{7}$$

The estimations of sub-critical crack behavior performed according to both methods are plotted in Fig. 12, for each stress level adopted in the fatigue tests. Thus, by using Eq. (3) with the parameters 'A^*' and 'n' calculated from Eqs. (5) and (6), the log–log straight lines 'v versus $K_{I,\max}$' of the first method are obtained. Individual values of crack growth rate (second method) are determined by using Eq. (7). In this case, for each point, the maximum stress intensity factor associated with crack growth rate is given by the relationship: $K_{I,\max}=(\sigma_{\max}/\sigma_{c,i})\times K_{IC}$. The obtained data points are also plotted in Fig. 12.

From the analysis of Fig. 12, a rough agreement is observed between the crack growth rate obtained by both estimation methods for both materials. According to these estimations, the subcritical crack growth occurred mainly at $K_{I,\max}$ values in the range of 3–5 MPa $m^{1/2}$ for the '97:03' material and in the range of 4–6 MPa $m^{1/2}$ for the '95:05' material. It is interesting to note that subcritical crack growth in human teeth takes place under stress intensity factors significantly lower than those observed for the artificial dental materials. However, one must also consider that natural teeth are not subjected to the same high stresses developed in abutment materials during mastication [23,24]. The main differences observed in the subcritical crack growth behavior of the materials are due to the higher number of long term fatigue tests (run-outs) verified for the '95:05' material. These results suggest that an improvement of the processing of specimen of the 95:05 composition would lead to considerable improvements of the fracture toughness and resistance to subcritical crack propagation.

The optimization of the sintering conditions of the '95:05' material, such as reduction of the initial bioglass particle size, increase of the milling/homogenization time, increase of the heating rate with a subsequent isothermal holding time, may lead to an improvement of the spreading of the glassy phase during sintering. As a result the number of pores and glass pockets in triple junctions may be reduced, promoting an increase of the mechanical properties.

4. Conclusions

Extremely fine grained and homogeneous 3Y-TZP ceramics with additions of 3 wt% and 5 wt% bioglass have been obtained at a sintering temperature as low as 1300 °C. Regardless of the content of bioglass added, the average grain size of zirconia was in the order of 0.30–0.35 μm. While hardness and fracture toughness of both compositions studied were quite similar, fracture strength of the 3Y-TZP material with 5 wt% bioglass was significantly lower, 360 MPa, compared to the material with 3 wt% bioglass, 450 MPa. Furthermore, a higher scattering of the strength values has been observed in the material with 5% glass addition, which is reflected in the lower Weibull modulus m of 5.6 in comparison to 7.2 for the material with 3 wt% bioglass. This difference in the mechanical properties is attributed to the higher amount of secondary intergranular phase and specifically to the formation of glass pockets at triple junctions. A more homogeneous distribution of the secondary bioglass phase may result in improved properties. The results indicate that the limit of fatigue strength with live times superior to 2×10^6 cycles is around 220 MPa for both materials studied, corresponding to about 50% of the static bending strength, 450 MPa, of

the 3Y-TZP–3% bioglass and about 65% of the static strength, 365 MPa, of the 3Y-TZP–5% bioglass. Based on these results, it is concluded that the material 3Y-TZP–3 wt% bioglass, sintered at 1300 °C is suitable for the preparation of long term structural components, considering its higher initial mechanical strength.

Acknowledgments

The authors acknowledge the FAPESP for financial support under Grant nos. 04/04386-1 and 05/52971-3.

References

[1] B.I. Ardlin, Transformation-toughened zirconia for dental inlays, crowns and bridges: chemical stability and effect of low-temperature aging on flexural strength and surface structure, Dental Materials 18 (2) (2002) 590–595.
[2] M. Guazatto, M. Albakry, S. Ringer, M.V. Swain, Strength, fracture toughness of all-ceramic materials. Part II—zirconia based dental ceramics, Dental Materials 20 (5) (2004) 449–456.
[3] D.-J. Kim, M.-H. Lee, D.Y. Lee, J.-S. Han, Mechanical properties, phase stability and biocompatibility of (Y,Nb)–TZP/Al_2O_3 composite abutments for dental implants, Journal of Biomedical Materials Research 53 (4) (2000) 438–443.
[4] X.-J. Sheng, H. Xu, Z.-H. Jin, Y.-L. Wang, Preparation of glass-infiltrated. 3Y-TZP/Al_2O_3/glass composites, Materials Letters 58 (11) (2004) 1750–1753.
[5] J.-M. Tian, Y.-L. Zhang, S.-X. Zhang, X.-P. Luo, Mechanical properties and microstructure of alumina–glass composites, Journal of the American Ceramic Society 82 (6) (1999) 1592–1594.
[6] R. Stevens, 2nd ed., An Introduction to Zirconia: Zirconia and Zirconia Ceramics, n.113, Magnesium Elektron Publications, Twickenham: Magnesium electrum, 1986.
[7] D. Basu, B.K. Sarkar, Toughness determination of zirconia toughened alumina ceramics from growth of indentation-induced cracks, Journal of Materials Research 11 (12) (1996) 3057–3062.
[8] B. Basu, J. Vlegels, O. Van Der Biest, Development of ZrO_2–TiB_2 composites: role of residual stress and starting powders, Journal of Alloys and Compounds 365 (1–2) (2004) 266–270.
[9] C. Piconi, G. Maccauro, Zirconia as a ceramic biomaterial, Biomaterials 20 (1999) 1–25.
[10] C. Piconi, W. Burger, H.G. Richter, A. Cittadini, Y-TZP ceramics for artificial joint replacements, Biomaterials 19 (16) (1998) 1489–1494.
[11] C. Santos, R.C. Souza, A.F. Habibe, L.D. Maeda, M.J.R. Barboza, C.N. Elias, Mechanical properties of Y-TZP ceramics obtained by liquid phase sintering, using bioglass as additive, Materials Science and Engineering: A 478 (2008) 257–263.
[12] Y.-H. Sun, Y.-F. Zhang, J.-K. Guo, Microstructure and bending strength of 3Y-TZP ceramics by liquid-phase sintering with CAS addition, Ceramics International 29 (2003) 229–232.
[13] X.W. Huang, S.W. Wang, X.X. Huang, Microstructure and mechanical properties of ZTA fabricated by liquid phase sintering, Ceramics International 29 (2003) 765–769.
[14] L.A. Bicalho, R.C. Souza, C. Santos, M.J.R. Barboza, C.A.R.P. Baptista, Fatigue of zirconia–bioglass dental ceramics, Materials Science Forum 591–593 (2008) 628–633.
[15] J.M. Oliveira, M.H. Fernandes, R.N. Correia, Development of a new glass-ceramic in the system MgO–3CaO · P_2O_5–SiO_2, Bioceramics 5 (1997) 7–14.
[16] J.M. Oliveira, R.N. Correia, M.H. Fernandes, Effects of Si speciation on the in vitro bioactivity of glasses, Biomaterials 23 (2) (2002) 371–379.
[17] G. Grathwohl, T. Liu, Crack resistance and fatigue of transforming ceramics: I, materials in the ZrO_2–Y_2O_3–Al_2O_3 system, Journal of the American Ceramic Society 74 (2) (1991) 318.
[18] G. Grathwohl, T. Liu, Crack resistance and fatigue of transforming ceramics: II, CeO_2-stabilized tetragonal ZrO_2, Journal of the American Ceramic Society 74 (12) (1991) 3028–3034.
[19] L.A. Bicalho, C. Santos, R.C. Souza, M.J.R. Barboza, C.A.R.P. Baptista, Mechanical behavior of ZrO_2–bioglass dental ceramics under cyclic fatigue loading, Materials Science Forum 636–637 (2010) 47–53.
[20] L.A. Bicalho, A.F. Habibe, C. Santos, M.J.R. Barboza, C.A.R.P. Baptista, Performance of ZrO_2–bioglass dental ceramics under cyclic fatigue loading, Cadernos UNIFOA 5 (2007) 30–33.
[21] R.C. Garvie, P.S. Nicholson, Phase analysis in zirconia systems, Journal of the American Ceramic Society 55 (1972) 303–305.
[22] W. Weibull, A statistical distribuition function of wide applicability, Journal of Applied Mechanics 18 (1951) 293–297.
[23] A.R. Studart, F. Filser, P. Kocher, H. Luthy, L.J. Gauckler, Cyclic fatigue in water of veneer-framework composites for all-ceramic dental bridges, Dental Materials 23 (2) (2007) 177–185.
[24] A.R. Studart, F. Filser, P. Kocher, L.J. Gauckleryuji Kimura, S. Takubo, In vitro lifetime of dental ceramics under cyclic loading in water, Biomaterials 28 (2007) 2695–2705.
[25] D. Munz, T. Fett, Ceramics—Mechanical Properties, Failure Behaviour, Materials Selection, Springer, 1998 303 p.
[26] J. Chevalier, C. Olagnon, G Fantozzi, Subcritical crack propagation in 3Y-TZP ceramics: static and cyclic fatigue, Journal of the American Ceramic Society 82 (11) (1999) 3129–3138.
[27] S.-Y. Liu, I.-W. Chen, Fatigue of yttria-stabilized Zirconia: II, crack propagation, fatigue striations, and short-crack behavior, Journal of the American Ceramic Society 74 (6) (1991) 1206–1216.
[28] A.R. Studart, F. Filser, P. Kocher, H. Luthy, L.J. Gauckler, Mechanical and fracture behavior of veneer-framework composites for all-ceramic dental bridges, Dental Materials 23 (1) (2006) 115–123.